Linear and nonlinear poroelastic AVO

Steven Kim and Kris Innanen

ABSTRACT

The purpose of our research is to merge the results of two recent theoretical and practical studies. First, Russell, and his fellow co-authors, has argued for a parameterization of the linearized AVO problem which highlights jumps in poroelastic properties across a reflecting boundary. The parameterization brings the Biot fluid term to the foreground. Second, Innanen has recently introduced an approach to analyzing linear and nonlinear AVO which mirrors the more general problem of scattering, and which accounts for low order nonlinearity in an intuitive way. This paper summarizes a project in which the poroelastic AVO problem is cast in terms of this nonlinear formalism. We derive first, second, and third order terms in an expansion for Rpp. The expansion is in terms of changes in density, shear modulus, and the Biot fluid term. We confirm mathematically the role second and third order fluid terms play in determining Rpp amplitudes. We comment on future directions the work can take, including moving towards a general poroelastic scattering picture, and incorporating dynamic poroelastic models also.

INTRODUCTION

As mentioned in the abstract, future research is expected to extend poroelastic AVO modeling methods to scattering theory (Weglein et al., 2003) and dynamic poroelastic models (Gurevich et al., 2004; and Cowin, 2013). In recent years, the geophysical community is showing interest in both of these categories. Scattering theorists have shown the benefits of Weglein-based methods (Weglein et al., 2009; Zhang et al., 2009; and Innanen et al., 2010). Dynamic poroelastic theory is discussed in detail to show that two compressional waves (a fast P-wave and a slow P-wave) and one shear wave is generated when an incoming P-wave, described as $e^{i\omega t}$ interacts with a geological boundary. This slow P-wave has lower amplitude and can be simulated in numerical simulations such as the work done by Arntsen (2001) where he models the microseismic events of a physical model that consists of a plate of unconsolidated sediment using Biot's theory, introducing stiffness and viscodynamic dissipation based on viscoelastic theory to model additional attenuation mechanisms.

Amplitude variation with offset (AVO) analysis of seismic reflections has become an important tool for hydrocarbon prospecting (Foster 2010). Various AVO parameterizations exist, all of which involve the sum of three weighted elastic-constant terms (Russell et al. 2011). Zoeppritz (1919) has provided the mathematical derivation for reflected and transmitted plane wave amplitudes which is the precursor that explains how AVO has evolved from it. The Zoeppritz equations provide exact values for reflected and transmitted plane waves in a 2D environment. However, the downside of the Zoeppritz equations is their highly complex nature of these equations which make interpretation of the amplitude data difficult. This includes the use of nonlinear techniques to estimate parameter values from the observed seismic amplitudes, which can be unstable (Russell et al. 2011).

The Zoeppritz equations used in this research are provided by Keys (1989). This formulation takes the form

$$\mathbf{P} \begin{bmatrix} R_{PP} \\ R_{PS} \\ T_{PP} \\ T_{PS} \end{bmatrix} = \mathbf{m}_P, \tag{1}$$

where **P** is a 4x4 matrix that contains sixteen elements. Each element is defined by elastic parameters V_P, V_S, and ρ. Here we have shown equation (1) in a condensed form to save space. Collapsing all of the weighting factors into A's will allow us to abbreviate each element in **P** so that

$$\mathbf{P} \equiv \begin{bmatrix} A_{11} & A_{12} & A_{13} & A_{14} \\ A_{21} & A_{22} & A_{23} & A_{24} \\ A_{31} & A_{32} & A_{33} & A_{34} \\ A_{41} & A_{42} & A_{43} & A_{44} \end{bmatrix}.$$

The vector on the right hand side of equation (1) is a vector containing four elements of a's that are also defined by elastic parameters V_P, V_S, and ρ and is shown in equation (2). Vector $\mathbf{m}_P$ four elements that appear as a column vector

$$\mathbf{m}_P = \begin{bmatrix} a_1 \\ a_2 \\ a_3 \\ a_4 \end{bmatrix}. \tag{2}$$

This version of the Zoeppritz equations will be further evaluated later in this paper to show we derive exact, linear, and nonlinear poroelastic AVO expressions. In order to demonstrate how to achieve these AVO expressions, the goal of this paper will be to: 1) Discuss Biot and Gassmann's poroelastic parameters 2) show the exact, linear, and nonlinear poroelastic AVO expressions in perturbation and reflectivity domains and 3) show results of numerical study using poroelastic AVO expressions. These three points are summarized by the following:

In the first step, we show that Biot (1941) and Gassmann (1951) have found a way to write bulk modulus (K), shear modulus (μ), and Lamé parameter (λ) under poroelastic conditions. This is shown by Russell et al. (2011) where they demonstrate how this is beneficial for AVO analysis.

In the second step, we achieve exact, linear, and nonlinear poroelastic AVO expressions for PP reflections. This requires a modification of the Zoeppritz equations where two substitutions need to take place. The first substitution is a transition from elastic constants (V_P, V_S, ρ) to poroelastic constants (f, μ, ρ) and the second transition is from poroelastic (f, μ, ρ) constants to perturbations (a_f, a_μ, a_ρ). This transition changes

the Zoeppritz equations into the poroelastic Zoeppritz equations in the perturbation domain. An application of Cramer's rule is performed such that the PP reflection coefficient, R_{PP}, can be isolated and an exact expression for poroelastic R_{PP} is a result. With the exact expression, a truncation of terms thus produces the linear and nonlinear poroelastic AVO approximations of R_{PP}. With this method, we may also produce exact, linear, and nonlinear expressions that are in terms of reflectivity parameters ($\Delta f / f$, $\Delta \mu / \mu$, $\Delta \rho / \rho$).

Once the exact, linear, and nonlinear poroelastic AVO expressions are found, a numerical study was performed for the set of poroelastic AVO expressions in the perturbation domain and reflectivity domain.

POROELASTICITY THEORY

Poroelasticity theory concerns what happens when we introduce a pore fluid into an initially dry (or drained) porous rock (Russell et al., 2011). Biot (1941) and Gassmann (1951) show that this pore fluid may be compensated by a fluid term ($f = \alpha^2 M$) that is the dissipative term corresponding to the viscoelastic effects associated with the squeezing of the fluid in the small, cracklike volumes surrounding the areas of contact (Biot, 1962). There are three elastic moduli that this theory applies to. The first modulus comes from the conclusion that Biot (1941) was able to acquire for the Lamé parameter λ where

$$\lambda_{\text{sat}} = \lambda_{\text{dry}} + \alpha^2 M \, , \tag{3}$$

the coefficient λ_{dry} represents the elastic compressibility due to the elastic grains, and $\alpha^2 M$ consists of the Biot coefficient (α) and poroelastic modulus. The second elastic modulus involves the bulk modulus that also compensates for fluid in the same way λ_{sat} can such that

$$K_{\text{sat}} = K_{\text{dry}} + \alpha^2 M \, , \tag{4}$$

The third and modulus involves the shear modulus and is unaffected by pore where

$$\mu_{\text{sat}} = \mu_{\text{dry}} \, . \tag{5}$$

Gassmann's (1951) contribution involves the Biot coefficient α and parameter M where both may be written in terms of elastic parameters.

Given the relations in equations (3), (4), and (5) the elastic equations for P-wave velocity and S-wave velocity may be rewritten such that they will account for poroelastic effects. For elastic media, expressions for P- and S-wave velocities can be written such that

$$V_P^2 = \frac{\lambda + 2\mu}{\rho} = \frac{K + (4/3)\mu}{\rho} = \frac{s}{\rho}, \tag{6}$$

and

$$V_S^2 = \frac{\mu}{\rho}, \tag{7}$$

where ρ is density and s is the 'skeleton' term (Russell et al., 2011). Biot (1941) and Gassmann (1951) have developed a fluid compensation mechanism that can be applied directly to elastic constants. This type of compensation is also known as a Gassmann fluid substitution. By using this substitution, we may transition the elastic P- and S-wave velocities into poroelastic P- and S-wave velocities by substituting equations (3), (4), and (5) into (6) and (7). We write these poroelastic expressions for V_P and V_S such that

$$\left(V_P\right)_{\text{sat}}^2 = \frac{\lambda_{\text{dry}} + 2\mu_{\text{sat}} + \alpha^2 M}{\rho_{\text{sat}}} = \frac{K_{\text{dry}} + (4/3)\mu_{\text{sat}} + \alpha^2 M}{\rho_{\text{sat}}}, \tag{8}$$

and

$$\left(V_S\right)_{\text{sat}}^2 = \frac{\mu_{\text{sat}}}{\rho_{\text{sat}}}. \tag{9}$$

Since equation (7) does not include the fluid modulus $\alpha^2 M$, the poroelastic S-wave velocity remains unchanged.

The poroelastic parameters as defined by Russell et al. (2011) are f, μ, and ρ. These parameters can be isolated from equations (8) and (9) where we may write f, μ, and ρ in terms of V_P, V_S, and ρ. We can then transition from these poroelastic parameters (f, μ, ρ) into perturbation parameters (a_f, a_μ, a_ρ) or reflectivity parameters ($\Delta f/f$, $\Delta\mu/\mu$, $\Delta\rho/\rho$). Perturbation and reflectivity notation is useful as they may be used as a dialing mechanism to measure relative change between two adjacent media. We may solve for a set AVO expressions either in terms of perturbation or reflectivity depending on the user preference. Thus, we may have two sets of equations that represent exact, linear, and nonlinear poroelastic AVO expressions.

In order to implement perturbation or reflectivity into the Zoeppritz equations, we must introduce the definitions for them. Perturbation terms for fluid, shear modulus, and density show the property contrasts of two adjacent media and are written such that

$$a_f = 1 - \frac{f_0}{f_1}, \quad a_\mu = 1 - \frac{\mu_0}{\mu_1}, \quad a_\rho = 1 - \frac{\rho_0}{\rho_1}. \tag{10}$$

The reflectivity terms are written differently

$$\frac{\Delta f}{f} = 2\frac{f_1 - f_0}{f_1 + f_0}, \qquad \frac{\Delta \mu}{\mu} = 2\frac{\mu_1 - \mu_0}{\mu_1 + \mu_0}, \qquad \frac{\Delta \rho}{\rho} = 2\frac{\rho_1 - \rho_0}{\rho_1 + \rho_0}, \qquad (11)$$

where each reflectivity term is a difference divided by the average. Equation (10) or (11), when substituted back into equation (1), will yield a new set of Zoeppritz equations that will effectively change all of the A_{ij} elements in **P** and a_j elements in $\mathbf{m}_P$. This new set of Zoeppritz equations will be referred to as the poroelastic Zoeppritz equations and are written as

$$\tilde{\mathbf{P}}\begin{bmatrix} \tilde{R}_{\mathrm{PP}} \\ \tilde{R}_{\mathrm{PS}} \\ \tilde{T}_{\mathrm{PP}} \\ \tilde{T}_{\mathrm{PS}} \end{bmatrix} = \tilde{\mathbf{m}}_P. \qquad (12)$$

The four-by-four matrix $\tilde{\mathbf{P}}$, containing a total of sixteen elements, is characterized by the poroelastic parameters f, μ, ρ and the incident angle of the P-wave, $\sin\theta_0$. The vector, $\tilde{\mathbf{m}}_P$, on the right hand side of equation (12) is a column vector of four elements that is characterized the same as $\tilde{\mathbf{P}}$. The details of $\tilde{\mathbf{P}}$ and $\tilde{\mathbf{m}}_P$ are shown in the appendix.

ACHIEVING EXACT, LINEAR, AND NONLINEAR $\tilde{R}_{\mathrm{PP}}$

After redefining each element of the Zoeppritz equations to account for poroelastic perturbation paameters, Cramer's rule is then implemented to solve for $\tilde{R}_{\mathrm{PP}}$. Doing so requires rearranging $\tilde{\mathbf{P}}$ in equation (12) such that another matrix is created. That is, it requires substituting the first column of $\tilde{A}_{ij}$ elements in $\tilde{\mathbf{P}}$ with the column of $\tilde{a}_j$ elements in $\tilde{\mathbf{m}}_P$. This new matrix will be called $\tilde{\mathbf{P}}_P$. The next step, according to Cramer's rule, is to calculate the determinant of matrices $\tilde{\mathbf{P}}_P$ and $\tilde{\mathbf{P}}$ and to take their quotient such that we can calculate PP reflection coefficient $\tilde{R}_{\mathrm{PP}}$ where

$$\tilde{R}_{\mathrm{PP}} = \frac{\det \tilde{\mathbf{P}}_P}{\det \tilde{\mathbf{P}}}. \qquad (13)$$

The solution for equation (13) is very large as it contains many instances of non-first order elements. The use of mathematical processing software Maple was useful to calculate the ratio of determinants for $\tilde{R}_{\mathrm{PP}}$, eliminate (cull) ordered terms that were unnecessary, and organize the algebra. There are two sets of approximations that bring the number of approximations to six: three that measure perturbation and another three that measure reflectivity. The first set of equations is shown in equations (14) – (16). These equations show the first, second, and third order approximations with respect to perturbations. In equation (14), the first order approximation shows three linear terms marked by a weighting coefficient, W, and a first order perturbation term. Equation (15) represents the second order approximation and contains the three linear terms from the first order approximation in addition to six second order terms that are also marked by a weighting coefficient and perturbations in second order. Equation (16) is the third order approximation contains a total of nineteen terms, ten of which are in third order. The second set of approximations, written with respect to reflectivity, is shown in equations

(17) – (19). This set of approximations contains the same number of ordered terms that is found in the equations representing perturbation.

In the set of approximations that measure perturbation, the first order approximation is

$$\tilde{R}_{\mathrm{PP}}\left(\theta_0\right)_1 = W_{a_1} a_f + W_{a_2} a_\mu + W_{a_3} a_\rho, \tag{14}$$

the second order approximation is

$$\begin{aligned}
\tilde{R}_{\mathrm{PP}}\left(\theta_0\right)_2 &= W_{a_1} a_f + W_{a_2} a_\mu + W_{a_3} a_\rho + W_{a_4} a_f^2 + W_{a_5} a_\mu^2 + W_{a_6} a_\rho^2 \\
&\quad + W_{a_7} a_f a_\mu + W_{a_8} a_f a_\rho + W_{a_9} a_\mu a_\rho,
\end{aligned} \tag{15}$$

and the third order approximation is

$$\begin{aligned}
\tilde{R}_{\mathrm{PP}}\left(\theta_0\right)_3 &= W_{a_1} a_f + W_{a_2} a_\mu + W_{a_3} a_\rho + W_{a_4} a_f^2 + W_{a_5} a_\mu^2 + W_{a_6} a_\rho^2 \\
&\quad + W_{a_7} a_f a_\mu + W_{a_8} a_f a_\rho + W_{a_9} a_\mu a_\rho + W_{a_{10}} a_f^3 + W_{a_{11}} a_\mu^3 + W_{a_{12}} a_\rho^3 \\
&\quad + W_{a_{13}} a_f^2 a_\mu + W_{a_{14}} a_f^2 a_\rho + W_{a_{15}} a_\mu^2 a_f + W_{a_{16}} a_\mu^2 a_\rho + W_{a_{17}} a_\rho^2 a_f \\
&\quad + W_{a_{18}} a_\rho^2 a_\mu + W_{a_{19}} a_f a_\mu a_\rho.
\end{aligned} \tag{16}$$

In the other set of approximations that measure reflectivity, the first order approximation is

$$\tilde{R}_{\mathrm{PP}}\left(\theta_0\right)_1 = W_{\Delta_1} \frac{\Delta f}{f} + W_{\Delta_2} \frac{\Delta \mu}{\mu} + W_{\Delta_3} \frac{\Delta \rho}{\rho}, \tag{17}$$

the second order approximation is

$$\begin{aligned}
\tilde{R}_{\mathrm{PP}}\left(\theta_0\right)_2 &= W_{\Delta_1} \frac{\Delta f}{f} + W_{\Delta_2} \frac{\Delta \mu}{\mu} + W_{\Delta_3} \frac{\Delta \rho}{\rho} + W_{\Delta_4} \left(\frac{\Delta f}{f}\right)^2 + W_{\Delta_5} \left(\frac{\Delta \mu}{\mu}\right)^2 \\
&\quad + W_{\Delta_6} \left(\frac{\Delta \rho}{\rho}\right)^2 + W_{\Delta_7} \frac{\Delta f}{f} \frac{\Delta \mu}{\mu} + W_{\Delta_8} \frac{\Delta f}{f} \frac{\Delta \rho}{\rho} + W_{\Delta_9} \frac{\Delta \mu}{\mu} \frac{\Delta \rho}{\rho},
\end{aligned} \tag{18}$$

and the third order approximation is

$$\tilde{R}_{PP}\left(\theta_0\right)_3 = W_{\Delta_1}\frac{\Delta f}{f} + W_{\Delta_2}\frac{\Delta \mu}{\mu} + W_{\Delta_3}\frac{\Delta \rho}{\rho} + W_{\Delta_4}\left(\frac{\Delta f}{f}\right)^2 + W_{\Delta_5}\left(\frac{\Delta \mu}{\mu}\right)^2$$

$$+ W_{\Delta_6}\left(\frac{\Delta \rho}{\rho}\right)^2 + W_{\Delta_7}\frac{\Delta f}{f}\frac{\Delta \mu}{\mu} + W_{\Delta_8}\frac{\Delta f}{f}\frac{\Delta \rho}{\rho} + W_{\Delta_9}\frac{\Delta \mu}{\mu}\frac{\Delta \rho}{\rho}$$

$$+ W_{\Delta_{10}}\left(\frac{\Delta f}{f}\right)^3 + W_{\Delta_{11}}\left(\frac{\Delta \mu}{\mu}\right)^3 + W_{\Delta_{12}}a_\rho^3\left(\frac{\Delta \rho}{\rho}\right)^3 + W_{\Delta_{13}}\left(\frac{\Delta f}{f}\right)^2\frac{\Delta \mu}{\mu} \quad (19)$$

$$+ W_{\Delta_{14}}\left(\frac{\Delta f}{f}\right)^2\frac{\Delta \rho}{\rho} + W_{\Delta_{15}}\left(\frac{\Delta \mu}{\mu}\right)^2\frac{\Delta f}{f} + W_{\Delta_{16}}\left(\frac{\Delta \mu}{\mu}\right)^2\frac{\Delta \rho}{\rho}$$

$$+ W_{\Delta_{17}}\left(\frac{\Delta \rho}{\rho}\right)^2\frac{\Delta f}{f} + W_{\Delta_{18}}\left(\frac{\Delta \rho}{\rho}\right)^2\frac{\Delta \mu}{\mu} + W_{\Delta_{19}}\frac{\Delta f}{f}\frac{\Delta \mu}{\mu}\frac{\Delta \rho}{\rho}.$$

The *W* coefficients in these two sets of approximations may be found in the appendix.

VALIDATION WITH RUSSELL AND GRAY

Russell and Gray have presented a linearized poroelastic approximation for PP reflection coefficients that resembles forms shown by Aki and Richards (2002), Shuey (1985), Wiggins et al. (1983), and Smith and Gidlow (1987). It is different from those mentioned by having the ability to detect fluid of the target of interest by predicting fluid directly from the amplitude data. Their equation takes the form

$$R_{PP}^{(RG)}\left(\theta\right) \approx \left[\left(1-\frac{\gamma_{dry}^2}{\gamma_{sat}^2}\right)\frac{\sec^2\theta}{4}\right]\frac{\Delta f}{f} + \left[\frac{\gamma_{dry}^2}{4\gamma_{sat}^2}\sec^2\theta - \frac{2}{\gamma_{sat}^2}\sin^2\theta\right]\frac{\Delta \mu}{\mu}$$

$$+ \left[\frac{1}{2} - \frac{\sec^2\theta}{4}\right]\frac{\Delta \rho}{\rho}, \quad (20)$$

where θ is the average between the incidence and refraction angles, $\Delta f/f$, $\Delta \mu/\mu$, $\Delta \rho/\rho$ are the reflectivities, $\gamma_{dry} = \left(V_{P_0} + V_{P_1}\right)_{dry}/\left(V_{S_0} + V_{S_1}\right)_{dry}$ and $\gamma_{sat} = \left(V_{P_0} + V_{P_1}\right)_{sat}/\left(V_{S_0} + V_{S_1}\right)_{sat}$, where the subscripts 'dry' and 'sat' represent the skeleton framework of the geologic matrix of the material and the skeleton framework that has been saturated in fluid, respectively. By comparing the first order approximation of $\tilde{R}_{PP}$ in reflectivity with the Russell and Gray approximation, we argue that this would validate our method. Our result yielded a first order approximation such that

$$\tilde{R}_{\text{PP}}\left(\theta_0\right)_1 = \left[\left(1 - \frac{\left(\gamma_0\right)_{\text{dry}}^2}{\left(\gamma_0\right)_{\text{sat}}^2}\right)\frac{\sec^2\theta_0}{4}\right]\frac{\Delta f}{f} + \left[\frac{\left(\gamma_0\right)_{\text{dry}}^2}{4\left(\gamma_0\right)_{\text{sat}}^2}\sec^2\theta_0 - \frac{2}{\left(\gamma_0\right)_{\text{sat}}^2}\sin^2\theta_0\right]\frac{\Delta\mu}{\mu}$$
$$+ \left[\frac{1}{2} - \frac{\sec^2\theta_0}{4}\right]\frac{\Delta\rho}{\rho}. \tag{21}$$

Equation (20) and (21) are relatively similar to each other in comparison. The only difference is the fact that the Russell and Gray approximation uses parameter averages instead of incident medium parameters for the first order approximation. This is explained by the two different approaches that are used to each equation (20) and (21). The Russell and Gray approximation is derived through the Aki and Richards approximation which, in itself, is parameterized by averages of the elastic properties V_P, V_S, ρ and average angle θ. The first order approximation is derivative of the Zoeppritz equations that is written in terms of elastic property components (V_{P_0}, V_{P_1}, V_{S_0}, V_{S_1}, ρ_0, ρ_1). By ultimately transforming the property components into perturbations, it was by choice to leave the parameters in terms of medium 0. The same form of AVO expressions, using our derivation technique, would result in the same form if we chose to involve parameters in terms of medium 1. Thus, equation (20) and (21) are equivalent.

NUMERICAL RESULTS

In figures (1) – (6), AVO modeling is performed on a model consisting of two homogeneous layers separated by a horizontal interface. The top layer (medium 0) contains its own unique set of fluid, shear modulus, and density parameters as does the bottom layer (medium 1). The numerical results are calculated such that fluid, shear modulus, and density are predetermined for medium 1. Depending on the level of contrast between medium 0 and medium 1 would be selected by the perturbation/reflectivity value. This value would then be used to calculate fluid, shear modulus, and density for medium 0.

This could also be done where medium 0 is used as the reference medium and the properties of medium 1 change relative to. For future work, we would need to consider emphasis on modeling AVO curves to match geophysically realistic properties.

For medium 1 the values selected are

$$f_1 = 7.000\,\text{GPa},$$
$$\mu_1 = 3.000\,\text{GPa},$$
$$\rho_1 = 2.200\,\text{g/cm}^3.$$

and medium 0 values are calculated using

$$f_0 = f_1\left(1 - a_f\right) = f_1\left(1 - \frac{\Delta f}{f}\left(1 + \frac{\Delta f}{2\Delta f}\right)^{-1}\right),$$

$$\mu_0 = \mu_1\left(1 - a_\mu\right) = \mu_1\left(1 - \frac{\Delta \mu}{\mu}\left(1 + \frac{\Delta \mu}{2\Delta \mu}\right)^{-1}\right),$$

$$\rho_0 = \rho_1\left(1 - a_\rho\right) = \rho_1\left(1 - \frac{\Delta \rho}{\rho}\left(1 + \frac{\Delta \rho}{2\Delta \rho}\right)^{-1}\right).$$

The AVO curves in figures (1) – (6) demonstrate the performance of the perturbation based equations and the reflectivity based equations. Figure (1) shows perturbation-based AVO modeling where all three perturbation constants are equal. Figure (2) shows reflectivity-based AVO modeling using where all three reflectivity constants are equal. In figures (3) – (5), a comparison is made between the perturbation and reflectivity models using perturbation/reflectivity constants that vary. By this we mean that we remain the perturbation/reflectivity constants to be equal and then to change the properties of either fluid, shear modulus, or density one at a time such that we can observe how this affects the amplitude trends as well as the accuracy of the approximations. Figure (6) continues to compare the performance of the perturbation models and the reflectivity models however, we select fluid, shear modulus, and density parameters such that medium property contrasts are equal instead of perturbation and reflectivity.

Figure (1) illustrates the capabilities of the perturbation approximations using values for a_f, a_μ, and a_ρ where the values are shown in table (1). Figure (1a) shows the reflection strengths based on small perturbation values $a_f = a_\mu = a_\rho = 0.100$. With these perturbation values, the first, second, and third order approximations are predicting exact $\tilde{R}_{PP}$ with high accuracy. Figure (1b) shows the reflection strengths based on a 0.1 increase in perturbation for each perturbation parameter such that $a_f = a_\mu = a_\rho = 0.200$. It is noticeable that the amplitude trend has increased due to the increase in perturbation. It is also apparent that the first order approximation has decreased in accuracy relative to exact $\tilde{R}_{PP}$. An increase in perturbation to $a_f = a_\mu = a_\rho = 0.400$ shows a more dramatic decrease in accuracy of the first order approximation as well as accuracy decrease for the second order approximation in figure (1c). In figure (1d), an increase of perturbation to $a_f = a_\mu = a_\rho = 0.500$ highlights a slight decrease in accuracy of the third order approximation.

Figures (2a) through (2d) illustrate the same numerical approach to model AVO curves as figures (1a) through (1d) by using $\frac{\Delta f}{f} = \frac{\Delta \mu}{\mu} = \frac{\Delta \rho}{\rho} = 0.100$ for figure (2a) and so on. Figure (2) measures the accuracy of the first, second, and third order approximations relative to exact $\tilde{R}_{PP}$ in the reflectivity domain ($\Delta f/f$, $\Delta \mu/\mu$, $\Delta \rho/\rho$). In figure (2a), the reflectivity parameters are small, $\frac{\Delta f}{f} = \frac{\Delta \mu}{\mu} = \frac{\Delta \rho}{\rho} = 0.100$. Reflectivity parameters of this magnitude show that the first, second, and third order approximations are predicting exact $\tilde{R}_{PP}$ very well. As reflectivity in fluid, shear modulus, and density is increased from

figure (2b) – (2d), the approximations do not lose any accuracy and maintain consistency with exact $\tilde{R}_{\text{PP}}$.

Figure (3) shows a comparison of the performance of the perturbation based modeling and the reflectivity based modeling simultaneously. (3a) and (3b) compare the differences in perturbation modeling and reflectivity modeling respectively using $a_f = \frac{\Delta f}{f} = 0.300$, $a_\mu = \frac{\Delta \mu}{\mu} = 0.100$, and $a_\rho = \frac{\Delta \rho}{\rho} = 0.100$. (3c) and (3d) compare the differences in perturbation and reflectively modeling respectively using $a_f = \frac{\Delta f}{f} = 0.100$, $a_\mu = \frac{\Delta \mu}{\mu} = 0.300$, and $a_\rho = \frac{\Delta \rho}{\rho} = 0.100$. (3e) and (3f) compare the difference in perturbation and reflectivity modeling respectively using $a_f = \frac{\Delta f}{f} = 0.100$, $a_\mu = \frac{\Delta \mu}{\mu} = 0.100$, and $a_\rho = \frac{\Delta \rho}{\rho} = 0.300$.

It is clear that comparing figures (3a) and (3b) shows that the first order approximation written for perturbation is less accurate than the first order approximation for reflectivity. In comparing figures (3c) and (3d), again the first order approximation in the perturbation domain is less accurate than the first order approximation in the reflectivity domain. For figures (3e) and (3f), the trend in the AVO curves is significantly different to the previous two sets of figures however; the result is similar in that the first order approximation in perturbation is less accurate than its reflectivity domain counterpart.

In figure (4), a similar type of analysis is performed as in (3). An increase in the single perturbation/reflectivity constant is measured to be 0.600. Doing so has significantly affected the accuracy of the first, second, and third order approximations in the perturbation domain. This is seen in figures (4a), (4c), and (4e). The reflectivity domain based equations however remain largely unaffected.

In figure (5), another increase in the single perturbation/reflectivity constant is now measured to be 0.900. This increase has brought another significant decrease in accuracy for first, second, and third order approximations measuring perturbations. The reflectivity based equations still maintain close proximity to the exact equations, especially for the nonlinear approximations.

In figure (6) the analysis is performed such that f, μ, and ρ for both the upper and lower media remain constant while a_f, a_μ, a_ρ and $\Delta f/f$, $\Delta\mu/\mu$, $\Delta\rho/\rho$ are calculated accordingly. In table (6), we notice that the perturbation values increase by increments of 0.200 from figure (6a) – (6c) and (6c) – (6e). The reflectivity values however, increase by 0.278 from figure (6b) – (6d) and another increase by 0.357 from figure (6d) – (6f). Given that the values for f, μ, and ρ are equally analyzed in each (6a), (6b), and (6c), (6d), and (6e), (6f) set, it is clear that the reflectivity domain equations are consistently more accurate than the perturbation based equations.
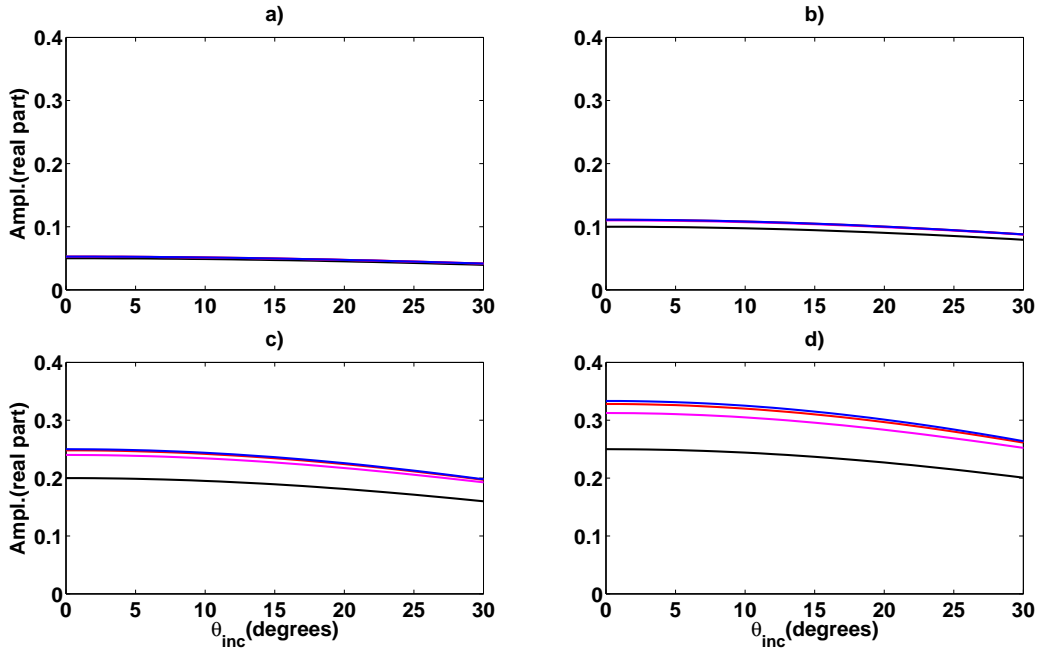
FIG. 1: All four panels have chosen a consistent perturbation each in a_f, a_μ, and a_ρ. There are four curves that are produced in each panel: the blue curve represents the exact solutions while the black, magenta, and red curve represents the 1st, 2nd, and 3rd order approximation respectively.

Figures	Values for perturbations $(a_f = a_\mu = a_\rho)$
5.1a	0.100
5.1b	0.200
5.1c	0.400
5.1d	0.500

TAB. 1: This displays the values used for perturbations from figure (1).
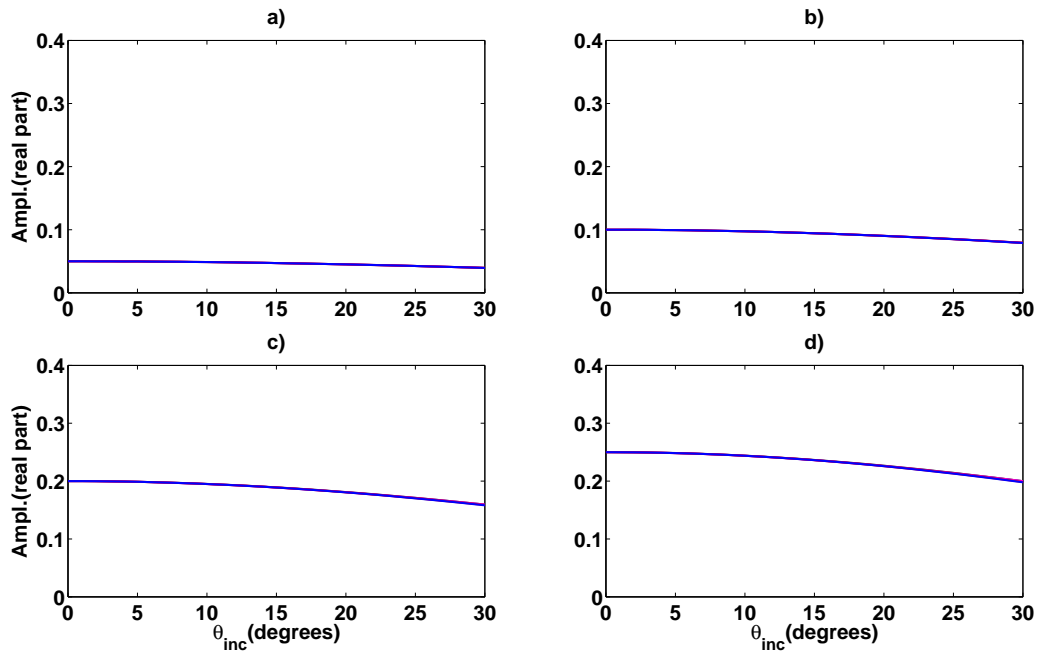
FIG. 2: All four panels have chosen a consistent reflectivity each in $\Delta f/f$, $\Delta \mu/\Delta \mu$, and $\Delta \rho/\rho$. There are four curves that are produced in each panel: the blue curve represents the exact solutions while the black, magenta, and red curve represents the 1st, 2nd, and 3rd order approximation respectively.

Figures	Values for perturbations $(\Delta f/f = \Delta \mu/\mu = \Delta \rho/\rho)$
5.2a	0.100
5.2b	0.200
5.2c	0.400
5.2d	0.500

TAB 2: This displays the values used for reflectivities from figure (2).
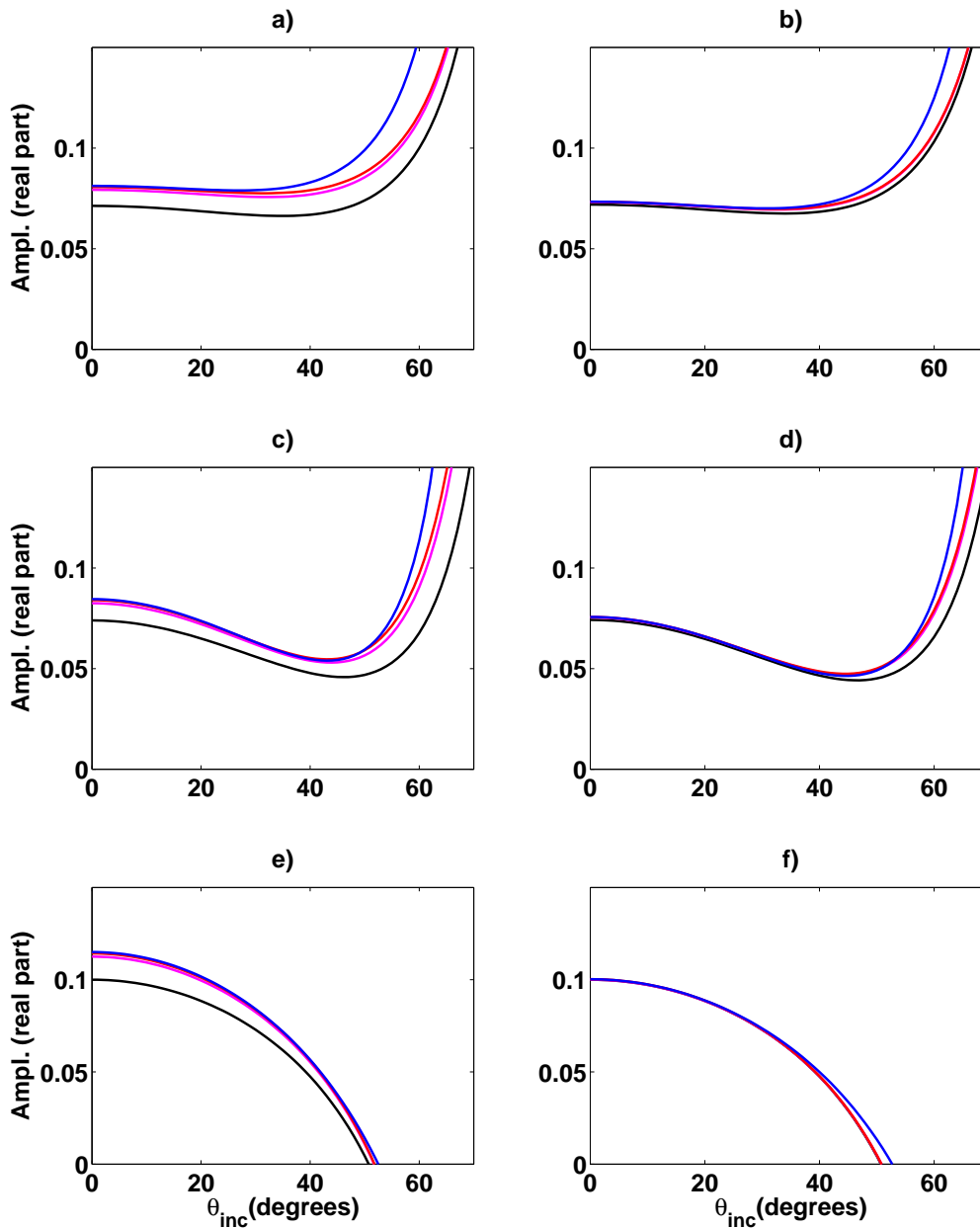
FIG. 3: (a), (c), and (e) represent the perturbation based poroelastic AVO approximations of 1st, 2nd, and 3rd order and are shown by the black, magenta, and red curves respectively. (b), (d), and (f) represent the reflectivity based poroelastic AVO approximations of 1st, 2nd, and 3rd order and are shown by the black, magenta, and red curves respectively. The exact amplitudes are shown by the blue curve.

Figure	a_f	a_μ	a_ρ	Figure	$\Delta f/f$	$\Delta\mu/\mu$	$\Delta\rho/\rho$
5.3a	0.300	0.100	0.100	5.3b	0.300	0.100	0.100
5.3c	0.100	0.300	0.100	5.3d	0.100	0.300	0.100
5.3c	0.100	0.100	0.300	5.3f	0.100	0.100	0.300

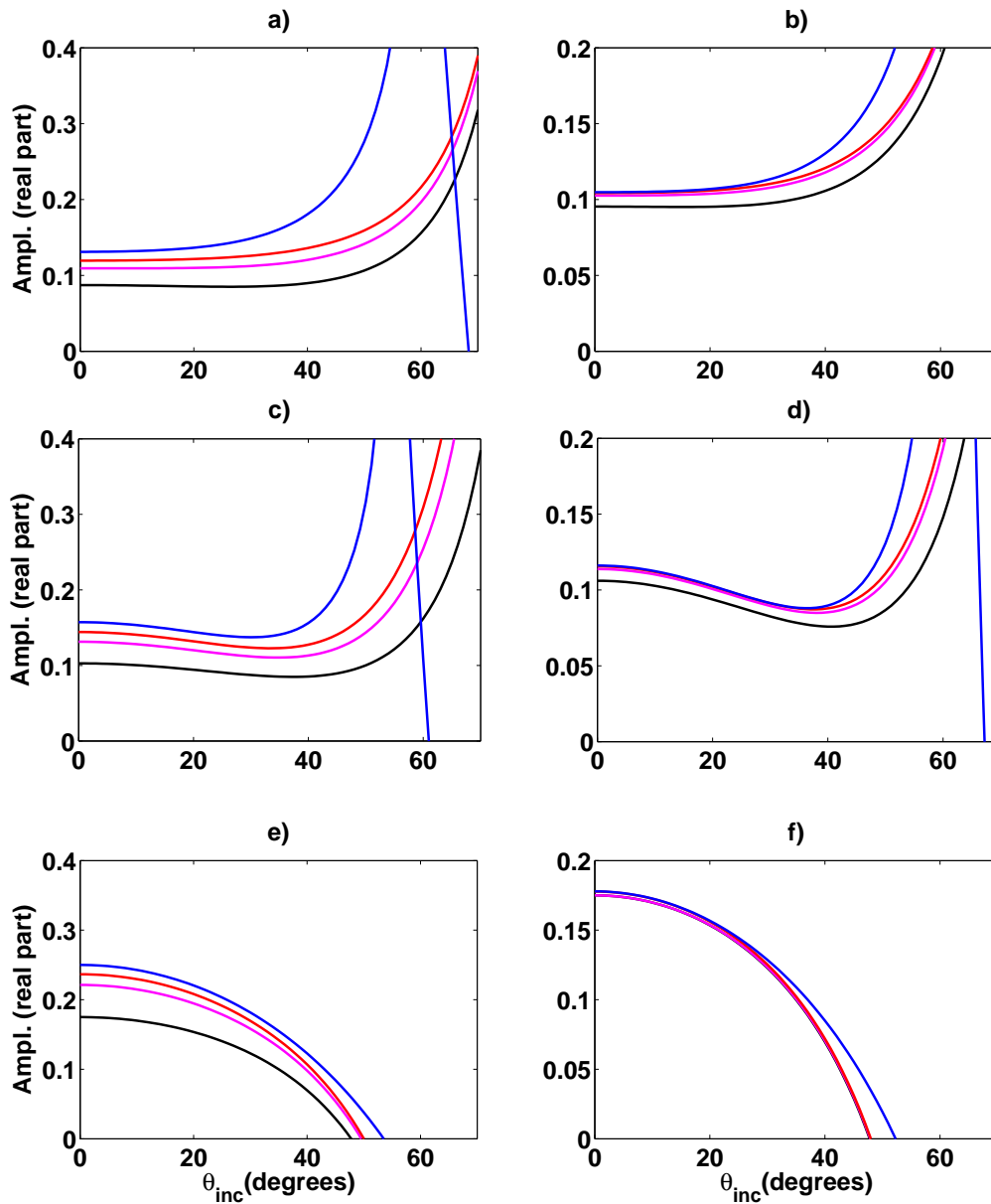TAB. 3: Values for perturbation and reflectivity for figure (3).

FIG. 4: (a), (c), and (e) represent the perturbation based poroelastic AVO approximations of 1st, 2nd, and 3rd order and are shown by the black, magenta, and red curves respectively. (b), (d), and (f) represent the reflectivity based poroelastic AVO approximations of 1st, 2nd, and 3rd order and are shown by the black, magenta, and red curves respectively. The exact amplitudes are shown by the blue curve.

Figure	a_f	a_μ	a_ρ	Figure	$\Delta f/f$	$\Delta\mu/\mu$	$\Delta\rho/\rho$
5.4a	0.600	0.100	0.100	5.4b	0.600	0.100	0.100
5.4c	0.100	0.600	0.100	5.4d	0.100	0.600	0.100
5.4c	0.100	0.100	0.600	5.4f	0.100	0.100	0.600

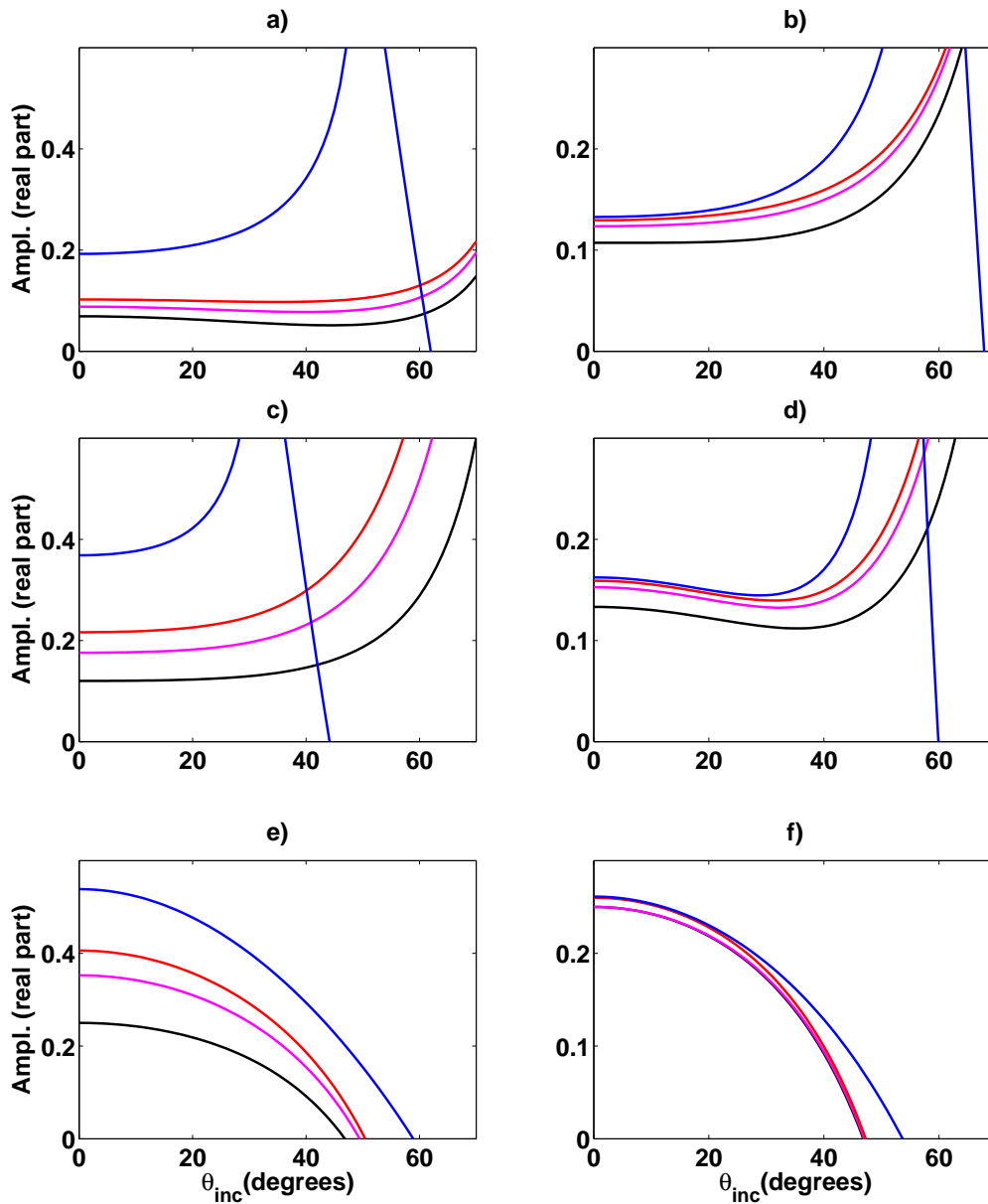TAB. 4: Values for perturbation and reflectivity for figure (4).

FIG. 5: (a), (c), and (e) represent the perturbation based poroelastic AVO approximations of 1st, 2nd, and 3rd order and are shown by the black, magenta, and red curves respectively. (b), (d), and (f) represent the reflectivity based poroelastic AVO approximations of 1st, 2nd, and 3rd order and are shown by the black, magenta, and red curves respectively. The exact amplitudes are shown by the blue curve.

Figure	a_f	a_μ	a_ρ	Figure	$\Delta f/f$	$\Delta\mu/\mu$	$\Delta\rho/\rho$
5.5a	0.900	0.100	0.100	5.5b	0.900	0.100	0.100
5.5c	0.100	0.900	0.100	5.5d	0.100	0.900	0.100
5.5c	0.100	0.100	0.900	5.5f	0.100	0.100	0.900

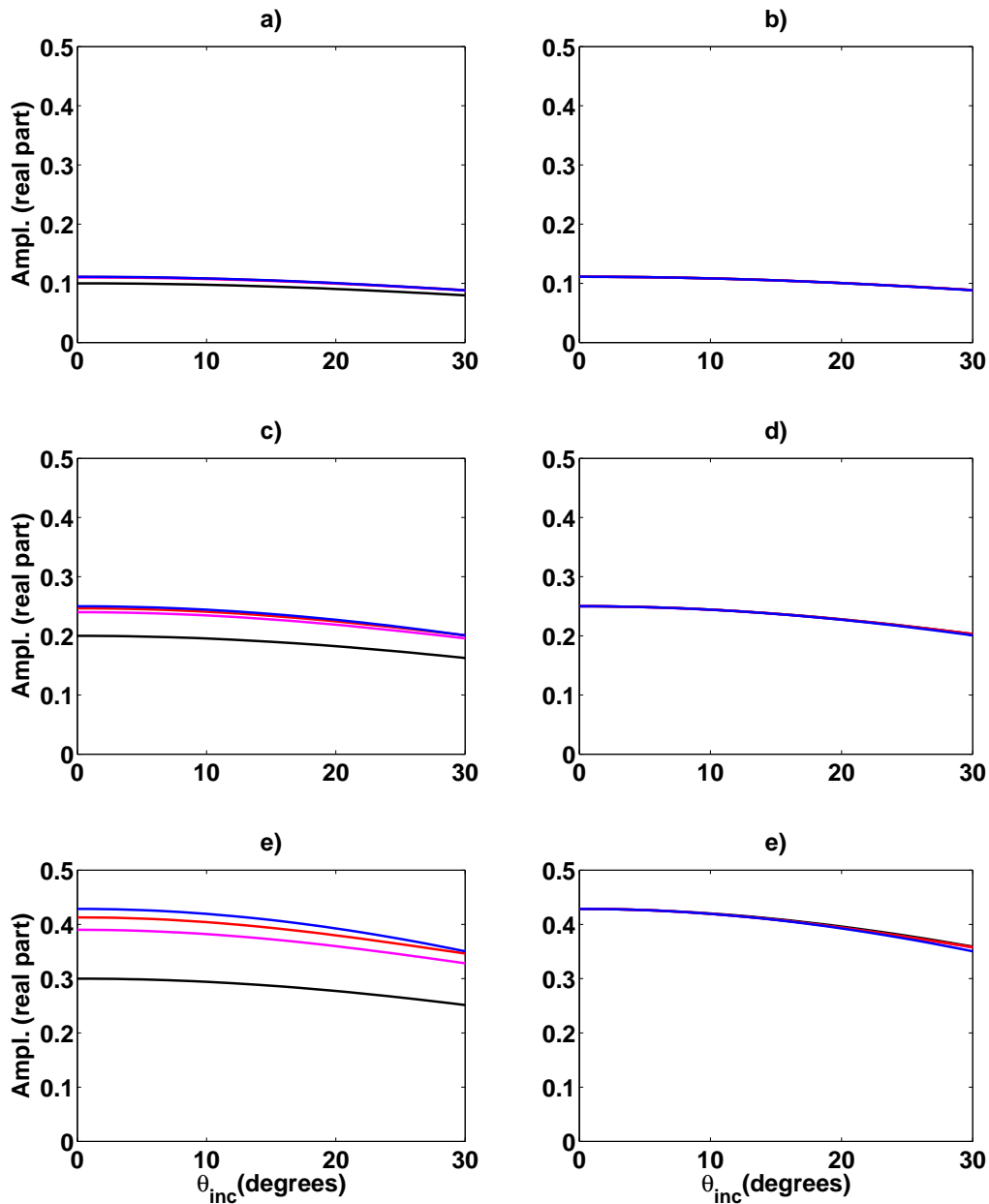TAB. 5: Values for perturbation and reflectivity for figure (5).

FIG. 6: (a), (c), and (e) represent the perturbation based poroelastic AVO approximations of 1st, 2nd, and 3rd order and are shown by the black, magenta, and red curves respectively. (b), (d), and (f) represent the reflectivity based poroelastic AVO approximations of 1st, 2nd, and 3rd order and are shown by the black, magenta, and red curves respectively. The exact amplitudes are shown by the blue curve.

Figure	a_f	a_μ	a_ρ	Figure	$\Delta f/f$	$\Delta\mu/\mu$	$\Delta\rho/\rho$
5.6a	0.200	0.200	0.200	5.6b	0.222	0.222	0.222
5.6c	0.400	0.400	0.400	5.6d	0.500	0.500	0.500
5.6c	0.600	0.600	0.600	5.6f	0.857	0.857	0.857

TAB. 6: Values for perturbation and reflectivity for figure (6).

CONCLUSIONS

Our method in deriving exact, linear, and nonlinear poroelastic AVO expressions come from manipulation of the Zoeppritz equations. This manipulation causes elastic parameters within the Zoeppritz equations to model poroelastic perturbation or poroelastic reflectivity instead. These poroelastic perturbation and reflectivity parameters stem from the work of Russell et al. (2011). Russell et al. (2011) provide an AVO expression that is able to account for fluids found in-situ. Using Biot (1941) and Gassmann (1951), Russell et al. (2011) are able to show how to compensate for pore fluids that are found in seismic amplitude data. We refer to this expression as the Russell and Gray approximation which is able to detect fluid directly from the amplitude data using a least squares technique. This approximation, however, only is able to account for amplitude variations for linear models. Thus, we have shown an alternate method to provide extensional benefit to account for nonlinearity that is typically found in AVO.

In our numerical study, it is clear that the results show that the ability to predict AVO data is better handled by the third order approximation. Moreover, the reflectivity domain approximations showed better predictions of AVO data than the perturbation domain approximations.

APPENDIX

The contents of this appendix show the weighting terms that are found in the first, second, and third order poroelastic AVO approximations for both in perturbation (a_f, a_μ, a_ρ) and reflectivity ($\Delta f/f$, $\Delta\mu/\mu$, $\Delta\rho/\rho$) domains. The weighting terms for perturbation are shown in sections (A.1) through (A.3) and the weighting terms for reflectivity are shown in sections (A.4) – (A.6). The elements of the poroelastic Zoeppritz equations for $\widetilde{\mathbf{P}}$ and $\widetilde{\mathbf{m}}_P$ are shown in section (A.7).

A.1 First order poroealstic weighting terms for a_f, a_μ, a_ρ

$$\tilde{R}_{\mathrm{PP}}^{(1)} = W_{a_1} a_f + W_{a_2} a_\mu + W_{a_3} a_\rho \tag{A.1}$$

$$W_{a_1} = \frac{1}{4}\left(1+\sin^2\theta_0\right) - \frac{(\gamma_0)_{\mathrm{dry}}^2}{4(\gamma_0)_{\mathrm{sat}}^2}\left(1+\sin^2\theta_0\right)$$

$$W_{a_2} = \frac{(\gamma_0)_{\mathrm{dry}}^2}{4(\gamma_0)_{\mathrm{sat}}^2}\left(1+\sin^2\theta_0\right) - \frac{2}{(\gamma_0)_{\mathrm{sat}}^2}\sin^2\theta_0$$

$$W_{a_3} = \frac{1}{4} - \frac{\sin^2\theta_0}{4}$$

A.2 Second order poroelastic weighting terms for a_f, a_μ, a_ρ

$$\tilde{R}_{\mathrm{PP}}^{(2)} = W_{a_4} a_f^2 + W_{a_5} a_\mu^2 + W_{a_6} a_\rho^2 + W_{a_7} a_f a_\mu + W_{a_8} a_f a_\rho + W_{a_9} a_\mu a_\rho \tag{A.2}$$

$$W_{a_4} = \left(1 - \frac{(\gamma_0)_{\mathrm{dry}}^2}{(\gamma_0)_{\mathrm{sat}}^2}\right)\frac{\sin^2\theta_0}{4} + \frac{1}{8}\left(1 - \frac{(\gamma_0)_{\mathrm{dry}}^4}{(\gamma_0)_{\mathrm{sat}}^4}\right)$$

$$W_{a_5} = \frac{(\gamma_0)_{\mathrm{dry}}^2}{4(\gamma_0)_{\mathrm{sat}}^2}\left(\sec^2\theta_0 - \frac{(\gamma_0)_{\mathrm{dry}}^2}{2(\gamma_0)_{\mathrm{sat}}^2}\right) - \frac{2}{(\gamma_0)_{\mathrm{sat}}^2}\left(1 - \frac{1}{2(\gamma_0)_{\mathrm{sat}}}\right)\sin^2\theta_0$$

$$W_{a_6} = \frac{1}{8}\left(1 - \frac{2}{(\gamma_0)_{\mathrm{sat}}}\sin^2\theta_0\right)$$

$$W_{a_7} = -\frac{(\gamma_0)_{\mathrm{dry}}^2}{4(\gamma_0)_{\mathrm{sat}}^2}\left(1 - \frac{(\gamma_0)_{\mathrm{dry}}^2}{(\gamma_0)_{\mathrm{sat}}^2}\right)$$

$$W_{a_8} = -\left(1 - \frac{(\gamma_0)_{\mathrm{dry}}^2}{(\gamma_0)_{\mathrm{sat}}^2}\right)\frac{\sin^2\theta_0}{4}$$

$$W_{a_9} = \frac{1}{(\gamma_0)_{\mathrm{sat}}^2}\left(1 - \frac{(\gamma_0)_{\mathrm{dry}}^2}{4}\right)\sin^2\theta_0$$

A.3 Third order poroelastic weighting terms for a_f, a_μ, a_ρ

$$\tilde{R}_{\text{PP}}^{(3)} = W_{a_{10}} a_f^3 + W_{a_{11}} a_\mu^3 + W_{a_{12}} a_\rho^3 + W_{a_{13}} a_f^2 a_\mu + W_{a_{14}} a_f^2 a_\rho + W_{a_{15}} a_\mu^2 a_f$$
$$+ W_{a_{16}} a_\mu^2 a_\rho + W_{a_{17}} a_\rho^2 a_f + W_{a_{18}} a_\rho^2 a_\mu + W_{a_{19}} a_f a_\mu a_\rho \tag{A.3}$$

$$W_{a_{10}} = \frac{1}{64}\left[5\left(1+3\sin^2\theta_0\right)\left(1-\frac{(\gamma_0)_{\text{dry}}^4}{5(\gamma_0)_{\text{sat}}^4}\right) + \frac{(\gamma_0)_{\text{dry}}^2}{(\gamma_0)_{\text{sat}}^2}\left(1-13\sin^2\theta_0\right) - 5\frac{(\gamma_0)_{\text{dry}}^6}{(\gamma_0)_{\text{sat}}^6}\left(1-\frac{\sin^2\theta_0}{5}\right) \right]$$

$$W_{a_{11}} = \frac{5}{64}\frac{(\gamma_0)_{\text{dry}}^6}{(\gamma_0)_{\text{sat}}^6}\left(1-\frac{\sin^2\theta_0}{5}\right) + \frac{(\gamma_0)_{\text{dry}}^2}{4(\gamma_0)_{\text{sat}}^2}\sec^2\theta_0 + \frac{7}{4(\gamma_0)_{\text{sat}}^3}\left(1-\frac{2(\gamma_0)_{\text{dry}}^2}{7(\gamma_0)_{\text{sat}}^2}\right)\sin^2\theta_0$$

$$-\frac{2}{(\gamma_0)_{\text{sat}}^2}\left(1-\frac{(\gamma_0)_{\text{dry}}^4}{16(\gamma_0)_{\text{sat}}^4}\right)\sin^2\theta_0 - \frac{(\gamma_0)_{\text{dry}}^4}{4(\gamma_0)_{\text{sat}}^4}$$

$$W_{a_{12}} = \frac{5}{64}\left(1+\frac{\sin^2\theta_0}{5}\right) - \frac{3}{16(\gamma_0)_{\text{sat}}}\sin^2\theta_0$$

$$W_{a_{13}} = \frac{15(\gamma_0)_{\text{dry}}^6}{64(\gamma_0)_{\text{sat}}^6}\left(1-\frac{\sin^2\theta_0}{5}\right) - \frac{(\gamma_0)_{\text{dry}}^2}{64(\gamma_0)_{\text{sat}}^2}\left(1+3\sin^2\theta_0\right) - \frac{7(\gamma_0)_{\text{dry}}^4}{32(\gamma_0)_{\text{sat}}^4}\left(1-\frac{3}{7}\sin^2\theta_0\right)$$

$$-\frac{(\gamma_0)_{\text{dry}}^2}{4(\gamma_0)_{\text{sat}}^4}\left(1-\frac{(\gamma_0)_{\text{dry}}^2}{2(\gamma_0)_{\text{sat}}^2}\right)\sin^2\theta_0 + \frac{1}{8(\gamma_0)_{\text{sat}}^2}\sin^2\theta_0$$

$$W_{a_{14}} = \frac{(\gamma_0)_{\text{dry}}^2}{32(\gamma_0)_{\text{sat}}^2}\left(1+9\sin^2\theta_0\right) - \frac{(\gamma_0)_{\text{dry}}^4}{64(\gamma_0)_{\text{sat}}^4}\sec^2\theta_0 - \frac{1}{64}\left(1+17\sin^2\theta_0\right)$$

$$W_{a_{15}} = \left(1-\frac{(\gamma_0)_{\text{dry}}^2}{(\gamma_0)_{\text{sat}}^2}\right)\left(\frac{(\gamma_0)_{\text{dry}}^2}{4(\gamma_0)_{\text{sat}}^4}-\frac{1}{2(\gamma_0)_{\text{sat}}^3}\right)\sin^2\theta_0 - \frac{(\gamma_0)_{\text{dry}}^2}{4(\gamma_0)_{\text{sat}}^2} + \frac{31(\gamma_0)_{\text{dry}}^4}{64(\gamma_0)_{\text{sat}}^4}\left(1-\frac{3}{31}\sin^2\theta_0\right)$$

$$-\frac{15(\gamma_0)_{\text{dry}}^6}{64(\gamma_0)_{\text{sat}}^6}\left(1-\frac{\sin^2\theta_0}{5}\right)$$

$$W_{a_{16}} = \frac{5}{4(\gamma_0)_{\text{sat}}^2}\left(1+\frac{(\gamma_0)_{\text{dry}}^2}{5(\gamma_0)_{\text{sat}}^2}\right)\sin^2\theta_0 - \frac{3}{4(\gamma_0)_{\text{sat}}^3}\left(1+\frac{(\gamma_0)_{\text{dry}}^2}{3(\gamma_0)_{\text{sat}}^{-1}}\right)\sin^2\theta_0 - \frac{(\gamma_0)_{\text{dry}}^4}{64(\gamma_0)_{\text{sat}}^4}\sec^2\theta_0$$

$$W_{a_{17}} = -\left(1-\frac{(\gamma_0)_{\text{dry}}^2}{(\gamma_0)_{\text{sat}}^2}\right)\left(\frac{1}{8(\gamma_0)_{\text{sat}}}+\frac{\sec^2\theta_0}{64}\right)$$

$$W_{a_{18}} = \frac{3}{8(\gamma_0)_{\text{sat}}^2}\left(1-\frac{(\gamma_0)_{\text{dry}}^2}{3(\gamma_0)_{\text{sat}}}\right)\sin^2\theta_0 - \frac{1}{16(\gamma_0)_{\text{sat}}}\sin^2\theta_0 - \frac{(\gamma_0)_{\text{dry}}^2}{64(\gamma_0)_{\text{sat}}^2}\sec^2\theta_0$$

$$W_{a_{19}} = \left(1 - \frac{(\gamma_0)^2_{\text{dry}}}{(\gamma_0)^2_{\text{sat}}} \right) \left(\frac{1}{4(\gamma_0)^2_{\text{sat}}} \sin^2 \theta_0 - \frac{(\gamma_0)^2_{\text{dry}}}{32(\gamma_0)^2_{\text{sat}}} \sec^2 \theta_0 \right)$$

A.4 First order poroelastic weighting terms for $\Delta f/f$, $\Delta\mu/\mu$, $\Delta\rho/\rho$

$$\tilde{R}^{(1)}_{\text{PP}} = W_{\Delta_1} \frac{\Delta f}{f} + W_{\Delta_2} \frac{\Delta\mu}{\mu} + W_{\Delta_3} \frac{\Delta\rho}{\rho} \tag{A.4}$$

$$W_{\Delta_1} = \left(1 - \frac{(\gamma_0)^2_{\text{dry}}}{(\gamma_0)^2_{\text{sat}}} \right) \frac{\sec^2 \theta_0}{4}$$

$$W_{\Delta_2} = \frac{(\gamma_0)^2_{\text{dry}}}{4(\gamma_0)^2_{\text{sat}}} \sec^2 \theta_0 - \frac{2}{(\gamma_0)^2_{\text{sat}}} \sin^2 \theta_0$$

$$W_{\Delta_3} = \frac{1}{2} - \frac{\sec^2 \theta_0}{4}$$

A.5 Second order poroelastic weighting terms for $\Delta f/f$, $\Delta\mu/\mu$, $\Delta\rho/\rho$

$$\tilde{R}^{(2)}_{\text{PP}} = W_{\Delta_4} \left(\frac{\Delta f}{f} \right)^2 + W_{\Delta_5} \left(\frac{\Delta\mu}{\mu} \right)^2 + W_{\Delta_6} \left(\frac{\Delta\rho}{\rho} \right)^2 + W_{\Delta_7} \frac{\Delta f}{f} \frac{\Delta\mu}{\mu} + W_{\Delta_8} \frac{\Delta f}{f} \frac{\Delta\rho}{\rho}$$
$$+ W_{\Delta_9} \frac{\Delta\mu}{\mu} \frac{\Delta\rho}{\rho} \tag{A.5}$$

$$W_{\Delta_4} = \frac{1}{8} \left(1 - \frac{(\gamma_0)^2_{\text{dry}}}{(\gamma_0)^2_{\text{sat}}} \right) \left(\sin^2 \theta_0 + \frac{(\gamma_0)^2_{\text{dry}}}{(\gamma_0)^2_{\text{sat}}} \right)$$

$$W_{\Delta_5} = \frac{(\gamma_0)^2_{\text{dry}}}{8(\gamma_0)^2_{\text{sat}}} \left(\sec^2 \theta_0 - \frac{(\gamma_0)^2_{\text{dry}}}{(\gamma_0)^2_{\text{sat}}} \right) - \frac{1}{(\gamma_0)^2_{\text{sat}}} \left(1 - \frac{1}{(\gamma_0)_{\text{sat}}} \right) \sin^2 \theta_0$$

$$W_{\Delta_6} = \left(1 - \frac{2}{(\gamma_0)_{\text{sat}}} \right) \frac{\sin^2 \theta_0}{8}$$

$$W_{\Delta_7} = -\frac{(\gamma_0)^2_{\text{dry}}}{4(\gamma_0)^2_{\text{sat}}} \left(1 - \frac{(\gamma_0)^2_{\text{dry}}}{(\gamma_0)^2_{\text{sat}}} \right)$$

$$W_{\Delta_8} = -\left(1 - \frac{(\gamma_0)^2_{\text{dry}}}{(\gamma_0)^2_{\text{sat}}} \right) \frac{\sin^2 \theta_0}{4}$$

$$W_{\Delta_9} = \frac{1}{(\gamma_0)^2_{\text{sat}}} \left(1 - \frac{(\gamma_0)^2_{\text{dry}}}{4} \right) \sin^2 \theta_0$$

A.6 Third order poroelastic weighting terms for $\Delta f/f$, $\Delta\mu/\mu$, $\Delta\rho/\rho$

$$\tilde{R}_{\text{PP}}^{(3)} = W_{\Delta_{10}}\left(\frac{\Delta f}{f}\right)^3 + W_{\Delta_{11}}\left(\frac{\Delta\mu}{\mu}\right)^3 + W_{\Delta_{12}}a_\rho^3\left(\frac{\Delta\rho}{\rho}\right)^3 + W_{\Delta_{13}}\left(\frac{\Delta f}{f}\right)^2\frac{\Delta\mu}{\mu}$$

$$+ W_{\Delta_{14}}\left(\frac{\Delta f}{f}\right)^2\frac{\Delta\rho}{\rho} + W_{\Delta_{15}}\left(\frac{\Delta\mu}{\mu}\right)^2\frac{\Delta f}{f} + W_{\Delta_{16}}\left(\frac{\Delta\mu}{\mu}\right)^2\frac{\Delta\rho}{\rho} \qquad (A.6)$$

$$+ W_{\Delta_{17}}\left(\frac{\Delta\rho}{\rho}\right)^2\frac{\Delta f}{f} + W_{\Delta_{18}}\left(\frac{\Delta\rho}{\rho}\right)^2\frac{\Delta\mu}{\mu} + W_{\Delta_{19}}\frac{\Delta f}{f}\frac{\Delta\mu}{\mu}\frac{\Delta\rho}{\rho}$$

$$W_{\Delta_{10}} = \frac{1}{64}\left[\begin{array}{c} 3\left(1 - \frac{(\gamma_0)_{\text{dry}}^4}{(\gamma_0)_{\text{sat}}^4}\right)\sin^2\theta_0 - 3\frac{(\gamma_0)_{\text{dry}}^2}{(\gamma_0)_{\text{sat}}^2}\left(1 + \frac{\sin^2\theta_0}{3}\right) + \left(1 + 7\frac{(\gamma_0)_{\text{dry}}^4}{(\gamma_0)_{\text{sat}}^4}\right) \\ -5\frac{(\gamma_0)_{\text{dry}}^6}{(\gamma_0)_{\text{sat}}^6}\left(1 - \frac{\sin^2\theta_0}{5}\right) \end{array}\right]$$

$$W_{\Delta_{11}} = \frac{5(\gamma_0)_{\text{dry}}^6}{64(\gamma_0)_{\text{sat}}^6}\left(1 - \frac{\sin^2\theta_0}{5}\right) - \frac{1}{2(\gamma_0)_{\text{sat}}^2}\left(1 + \frac{(\gamma_0)_{\text{dry}}^2}{(\gamma_0)_{\text{sat}}^3}\right)\sin^2\theta_0 + \frac{(\gamma_0)_{\text{dry}}^2}{16(\gamma_0)_{\text{sat}}^2}\sec^2\theta_0$$

$$- \frac{(\gamma_0)_{\text{dry}}^4}{8(\gamma_0)_{\text{sat}}^4}\left(1 - \frac{\sin^2\theta_0}{(\gamma_0)_{\text{sat}}^2}\right) + \frac{3}{4(\gamma_0)_{\text{sat}}^3}\sin^2\theta_0$$

$$W_{\Delta_{12}} = \frac{1}{64}\left(1 - 3\sin^2\theta_0\right) + \frac{1}{16(\gamma_0)_{\text{sat}}}\sin^2\theta_0$$

$$W_{\Delta_{13}} = \frac{1}{8(\gamma_0)_{\text{sat}}^2}\sin^2\theta_0 - \frac{3(\gamma_0)_{\text{dry}}^2}{64(\gamma_0)_{\text{sat}}^2}\left(1 + \frac{(\gamma_0)_{\text{dry}}^4}{(\gamma_0)_{\text{sat}}^4}\right)\sin^2\theta_0 - \frac{(\gamma_0)_{\text{dry}}^2}{4(\gamma_0)_{\text{sat}}^4}\left(1 - \frac{(\gamma_0)_{\text{dry}}^2}{2(\gamma_0)_{\text{sat}}^2}\right)\sin^2\theta_0$$

$$- \frac{11(\gamma_0)_{\text{dry}}^4}{32(\gamma_0)_{\text{sat}}^4}\left(1 - \frac{3}{11}\sin^2\theta_0\right) + \frac{7(\gamma_0)_{\text{dry}}^2}{64(\gamma_0)_{\text{sat}}^2}\left(1 + \frac{15(\gamma_0)_{\text{dry}}^4}{7(\gamma_0)_{\text{sat}}^4}\right)$$

$$W_{\Delta_{14}} = \frac{(\gamma_0)_{\text{dry}}^2}{32(\gamma_0)_{\text{sat}}^2}\left(1 + 5\sin^2\theta_0\right) - \frac{(\gamma_0)_{\text{dry}}^4}{64(\gamma_0)_{\text{sat}}^4}\sec^2\theta_0 - \frac{1}{64}\left(1 + 9\sin^2\theta_0\right)$$

$$W_{\Delta_{15}} = \left(\frac{(\gamma_0)_{\text{dry}}^2}{4(\gamma_0)_{\text{sat}}^4} - \frac{1}{2(\gamma_0)_{\text{sat}}^3}\right)\left(1 - \frac{(\gamma_0)_{\text{dry}}^2}{(\gamma_0)_{\text{sat}}^2}\right)\sin^2\theta_0 - \frac{15(\gamma_0)_{\text{dry}}^6}{64(\gamma_0)_{\text{sat}}^6}\left(1 - \frac{3}{15}\sin^2\theta_0\right)$$

$$+ \frac{23(\gamma_0)_{\text{dry}}^4}{64(\gamma_0)_{\text{sat}}^4}\left(1 - \frac{3}{23}\sin^2\theta_0\right) - \frac{(\gamma_0)_{\text{dry}}^2}{8(\gamma_0)_{\text{sat}}^2}$$

$$W_{\Delta_{16}} = \frac{3}{4(\gamma_0)_{\text{sat}}^2}\left(1 - \frac{1}{(\gamma_0)_{\text{sat}}}\right)\sin^2\theta_0 - \frac{(\gamma_0)_{\text{dry}}^2}{8(\gamma_0)_{\text{sat}}^2}\left(1 - \frac{2}{(\gamma_0)_{\text{sat}}^2}\right)\sin^2\theta_0 - \frac{(\gamma_0)_{\text{dry}}^4}{64(\gamma_0)_{\text{sat}}^4}\sec^2\theta_0$$

$$W_{\Delta_{17}} = \left(1 - \frac{(\gamma_0)^2_{\text{dry}}}{(\gamma_0)^2_{\text{sat}}}\right)\left(\frac{9}{64}\sin^2\theta_0 - \frac{1}{8(\gamma_0)_{\text{sat}}}\sin^2\theta_0 - \frac{1}{64}\right)$$

$$W_{\Delta_{18}} = -\frac{(\gamma_0)^2_{\text{dry}}}{64(\gamma_0)^2_{\text{sat}}}\left(1 - 9\sin^2\theta_0\right) - \frac{1}{16(\gamma_0)_{\text{sat}}}\left(1 + 2\frac{(\gamma_0)^2_{\text{dry}}}{(\gamma_0)^2_{\text{sat}}}\right)\sin^2\theta_0 - \frac{1}{8(\gamma_0)^2_{\text{sat}}}\sin^2\theta_0$$

$$W_{\Delta_{19}} = \left(1 - \frac{(\gamma_0)^2_{\text{dry}}}{(\gamma_0)^2_{\text{sat}}}\right)\left(\frac{\sin^2\theta_0}{4(\gamma_0)^2_{\text{sat}}} - \frac{(\gamma_0)^2_{\text{dry}}}{32(\gamma_0)^2_{\text{sat}}}\sec^2\theta_0\right)$$

A.7 Elements for $\widetilde{\mathbf{P}}$ and $\widetilde{\mathbf{m}}_P$ in the poroelastic Zoeppritz equations

From equation (12), we write the $\tilde{A}_{ij}$ elements of $\widetilde{\mathbf{P}}$ such that

$$\widetilde{\mathbf{P}} \equiv \begin{bmatrix} \tilde{A}_{11} & \tilde{A}_{12} & \tilde{A}_{13} & \tilde{A}_{14} \\ \tilde{A}_{21} & \tilde{A}_{22} & \tilde{A}_{23} & \tilde{A}_{24} \\ \tilde{A}_{31} & \tilde{A}_{32} & \tilde{A}_{33} & \tilde{A}_{34} \\ \tilde{A}_{41} & \tilde{A}_{42} & \tilde{A}_{43} & \tilde{A}_{44} \end{bmatrix},$$

For $\widetilde{\mathbf{m}}_P$, we write the $\tilde{a}_j$ elements as a column vector where

$$\widetilde{\mathbf{m}}_P = \begin{bmatrix} \tilde{a}_1 \\ \tilde{a}_2 \\ \tilde{a}_3 \\ \tilde{a}_4 \end{bmatrix}.$$

We will display each $\tilde{A}_{ij}$ element of $\widetilde{\mathbf{P}}$ row-by-row and each $\tilde{a}_j$ in $\widetilde{\mathbf{m}}_P$ respectively in terms of poroelastic perturbations a_f, a_μ, a_ρ. Note that matrix $\widetilde{\mathbf{P}}$ and column vector $\widetilde{\mathbf{m}}_P$ may be written in terms of poroelastic reflectivities $\Delta f/f$, $\Delta \mu/\mu$, $\Delta \rho/\rho$. In the first row $\widetilde{\mathbf{P}}$, the $\tilde{A}_{ij}$ elements are

$$\tilde{A}_{11} = -\sin\theta_0,$$

$$\tilde{A}_{12} = -\left[1 - (\gamma_0)^2_{\text{sat}}\sin^2\theta_0\right]^{1/2},$$

$$\tilde{A}_{13} = \left(\frac{(\gamma_0)^2_{\text{dry}}}{(\gamma_0)^2_{\text{sat}}}\frac{(1-a_\rho)}{(1-a_\mu)} + \left(1 - \frac{(\gamma_0)^2_{\text{dry}}}{(\gamma_0)^2_{\text{sat}}}\right)\frac{(1-a_\rho)}{(1-a_f)}\right)^{1/2}\sin\theta_0,$$

$$\tilde{A}_{14} = -\left[1 - \frac{(1-a_\mu)^{-1}(1-a_\rho)}{(\gamma_0)^2_{\text{sat}}}\sin^2\theta_0\right]^{1/2},$$

the elements of the second row are

$$\tilde{A}_{21} = \left[1 - \sin^2\theta_0\right]^{1/2},$$

$$\tilde{A}_{22} = -(\gamma_0)_{\text{sat}}\sin\theta_0,$$

$$\tilde{A}_{23} = \left[1 - \left\{ (1-a_\rho) \left[\left(\frac{(\gamma_0)^2_{\text{dry}}}{(\gamma_0)^2_{\text{sat}}} \right) (1-a_\mu)^{-1} + \left(1 - \frac{(\gamma_0)^2_{\text{dry}}}{(\gamma_0)^2_{\text{sat}}} \right) (1-a_f)^{-1} \right] \right\} \sin^2 \theta_0 \right]^{1/2} ,$$

$$\tilde{A}_{24} = \frac{\left((1-a_\mu)^{-1} (1-a_\rho) \right)^{1/2}}{(\gamma_0)_{\text{sat}}} \sin \theta_0 ,$$

the elements of the third row are

$$\tilde{A}_{31} = 2 (\gamma_0)^2_{\text{sat}} \sin \theta_0 \left[1 - \sin^2 \theta_0 \right]^{1/2} ,$$

$$\tilde{A}_{32} = (\gamma_0)_{\text{sat}} \left[1 - 2 (\gamma_0)^2_{\text{sat}} \sin^2 \theta_0 \right] ,$$

$$\tilde{A}_{33} = 2 (1-a_\rho)^{-1} \left(\frac{(1-a_\mu)^{-1} (1-a_\rho)}{(\gamma_0)^2_{\text{sat}}} \right) \sin \theta_0$$

$$\times \left[1 - \left((1-a_\rho) \left[\left(\frac{(\gamma_0)^2_{\text{dry}}}{(\gamma_0)^2_{\text{sat}}} \right) (1-a_\mu)^{-1} + \left(1 - \frac{(\gamma_0)^2_{\text{dry}}}{(\gamma_0)^2_{\text{sat}}} \right) (1-a_f)^{-1} \right] \right) \sin^2 \theta_0 \right]^{1/2} ,$$

$$\tilde{A}_{34} = - (1-a_\rho)^{-1} \left(\frac{(1-a_\mu)^{-1} (1-a_\rho)}{(\gamma_0)^2_{\text{sat}}} \right)^{1/2} \left[1 - 2 \left(\frac{(1-a_\mu)^{-1} (1-a_\rho)}{(\gamma_0)^2_{\text{sat}}} \right) \sin^2 \theta_0 \right] ,$$

the elements of the fourth row are

$$\tilde{A}_{41} = - \left[1 - 2 (\gamma_0)^2_{\text{sat}} \sin^2 \theta_0 \right] ,$$

$$\tilde{A}_{42} = 2 (\gamma_0)^2_{\text{sat}} \sin \theta_0 \left[1 - (\gamma_0)^2_{\text{sat}} \sin^2 \theta_0 \right]^{1/2} ,$$

$$\tilde{A}_{43} = (1-a_\rho)^{-1} \left\{ (1-a_\rho) \left[\left(\frac{(\gamma_0)^2_{\text{dry}}}{(\gamma_0)^2_{\text{sat}}} \right) (1-a_\mu)^{-1} + \left(1 - \frac{(\gamma_0)^2_{\text{dry}}}{(\gamma_0)^2_{\text{sat}}} \right) (1-a_f)^{-1} \right] \right\}^{1/2}$$

$$\times \left[1 - 2 \left(\frac{(1-a_\mu)^{-1} (1-a_\rho)}{(\gamma_0)^2_{\text{sat}}} \right) \sin^2 \theta_0 \right] ,$$

$$\tilde{A}_{44} = 2 (1-a_\rho)^{-1} \left(\frac{(1-a_\mu)^{-1} (1-a_\rho)}{(\gamma_0)^2_{\text{sat}}} \right) \sin \theta_0 \left[1 - \left(\frac{(1-a_\mu)^{-1} (1-a_\rho)}{(\gamma_0)^2_{\text{sat}}} \right) \sin^2 \theta_0 \right]^{1/2} ,$$

and the elements of the vector, $\tilde{\mathbf{m}}_P$, on the right-hand side are

$$\tilde{a}_1 = \sin \theta_0 ,$$

$$\tilde{a}_2 = \left[1 - \sin^2 \theta_0 \right]^{1/2} ,$$

$$\tilde{a}_3 = 2 (\gamma_0)^2_{\text{sat}} \sin \theta_0 \left[1 - \sin^2 \theta_0 \right]^{1/2} ,$$

$$\tilde{a}_4 = \left[1 - 2 (\gamma_0)^2_{\text{sat}} \sin^2 \theta_0 \right] .$$

In the Zoeppritz equations shown in equation (1), there are instances of V_P/V_S ratios that occur. These ratios are replaced with the parameter γ in equation (12). We also used the subscript '0' to indicate that the parameter is referencing the upper medium of a two-layer model.

REFERENCES

Aki, K., and Richards, P. G., 2002, Quantitative seismology, 2nd ed: W. H. Freeman and Co.

Arntsen, B., Carcione, J. M., 2001, Numerical simulation of the Biot slow wave in water-saturated Nivelsteiner Sandstone: Geophysics, **66**, 890-896.

Biot, M. A., 1941, General theory of three-dimensional consolidation: Applied Physics, **12**, 155-164

Biot, M. A., 1962, Mechanics of deformation and acoustic propagation in porous media: Applied Physics, **33**, 1482-1498.

Cowin S. C., 2013, Continuum mechanics of anisotropic materials: Springer Science+Business Media New York.

Foster, D. J., Keys, R. G., and Lane, F. D., 2010, Interpretation of AVO anomalies: Geophysics, **75**, 75A3-75A13.

Gassmann, F., 1951, Über die elastizitat poroser median: Vierteljahrsschrift der naturforschenden gesellschaft, **96**.

Gurevich, B., Ciz, R., and Denneman A. I. M., 2004, Simple expressions for normal incidence reflection coefficients from an interface between fluid-saturated porous materials: Geophysics, **69**, 1372-1377.

Innanen, K. A., and Lira, J. E., 2010, Direct nonlinear Q-compensation of seismic primaries reflecting from a stratified, two-parameter absorptive medium: Geophysics, **75**, V13-V23.

Keys, R. G., 1989, Polarity reversals in reflections from layered media: Geophysics, **54**, 900-905.

Russell, B. H., Gray, D., and Hampson, D. P., 2011, Linearized AVO and poroelasticity: Geophysics, **76**, C19-C29.

Shuey, R., 1985, A simplification of the Zoeppritz equations: Geophysics, **50**, 609-614.

Smith, G., and Gidlow, P., 1987, Weighted stacking for rock property estimation and detection of gas: Geophysical Prospecting, **35**, 993-1014.

Weglein, A. B., Fernanda, V. A., Carvalho, P. M., Stolt, R. H., Matson, K. H., Coates, R. T., Corrigan, D., Foster, D. J., Shaw, S. A., and Zhang, H., 2003, Inverse scattering series and seismic exploration: Inverse Problems, **19**, R27-R83

Weglein, A. B., Zhang, H., Ramirez, A. C., Liu, F., and Lira, J. E. M., 2009, Clarifying the underlying and fundamental meaning of the approximate linear inversion of seismic data: Geophysics, **74**, WCD1-WCD13.

Wiggins, R., Kenny, G. S., and McClure, C. D., 1983, A method for determining and displaying the shear-velocity reflectivities of a geologic formation: European Patent Application 0113944.

Zhang, H., Weglein, A. B., 2009, Direct nonlinear inversion of 1D acoustic media using inverse scattering subseries: Geophysics, 74, WCD29-WCD39.

Zoeppritz, K,. 1919, Erdbebenwellen VIII B, Über die Reflexion und Durchgangseismischer Wellen durch Unstetigkeitsflächen: Gottinger Nachr, **1**, 66–84.